Received: 1 October 2021 | Revised: 28 October 2021 | Accepted: 29 October 2021

DOI: 10.1002/pol.20210737

RESEARCH ARTICLE

JOURNAL OF POLYMER SCIENCE WILEY

Mechanisms of ion transport in lithium salt-doped polymeric ionic liquid electrolytes at higher salt concentrations

Zidan Zhang | **Dachey Lin** | **Venkat Ganesan**

McKetta Department of Chemical Engineering, University of Texas at Austin, Austin, Texas, USA

Correspondence
Venkat Ganesan, McKetta Department of Chemical Engineering, University of Texas at Austin, Austin, Texas 78712, USA.
Email: venkat@che.utexas.edu

Funding information
National Science Foundation, Division of Materials Research, Grant/Award Number: 1721512; Welch Foundation, Grant/Award Number: F1599

Abstract

We used atomistic simulations to study the mechanisms of ion transport in salt-doped polymeric ionic liquid systems at higher salt concentrations. Consistent with the experimental observations, our simulations indicate that at higher salt concentrations, the anion mobilities become lower than that of the lithium cations. Further, the anion mobilities become relatively insensitive to the salt concentration, while the mobilities of lithium increase with increasing salt concentration. We rationalize the results for the anion mobilities by considering the fractions of anions which are exclusively coordinated with the polycations (Type1); co-coordinated with cations and lithium (Type2); and those exclusively coordinated with lithium (Type3). By considering the coordination characteristics of the different types of anions and their hopping motions, we demonstrate that the net anion mobilities results from a compensation effect of the salt concentration dependence of the mobilities of the different anions. With respect to the mobilities of the lithium ions, we demonstrate that the latter moves primarily by a structural diffusion mechanism involving refreshing of the solvation shell during hopping. Further, for the majority of the lithium ions, the solvation shell is shown to be comprised of co-coordinated Type2 anions, and that the number of polycations and the unique polymer chains involved in such coordination decreases with increasing salt concentration. Such changes are shown to weaken the solvation shell around the lithium, thereby facilitating faster ion motion. Together, our results suggest that systems in which the anion which exhibits a stronger coordination to the polycation in comparison to that of the lithium can facilitate higher transference numbers without a concomitant reduction in the mechanical strength.

KEYWORDS

concentration, conducting materials, diffusion, lithium salt, polymeric ionic liquid, transport

1 | INTRODUCTION

Solid polymer electrolytes (SPEs) are emerging as promising candidates for lithium ion batteries (LIBs) as means to overcome issues relating to flammability, liquid electrolyte leakage, dendrite formation, low thermal stability, poor mechanical properties and toxicity.[1,2] As a family member of SPEs, polymeric ionic liquids (polyIL) that use traditional ionic liquid ions as their repeating units have been shown to possess low glass transition

temperature (T_g) with high charge densities.[3–8] However, as a result of tethering the counterion to the polymer backbone, polyILs exhibit lower ionic conductivities even relative to other salt-doped SPEs.[1,9–20] Hence, a number of efforts have been exploring strategies such as block copolymer polyILs,[21–31] plasticizing polyILs using ILs,[32,33] salt doping polyILs[31,34–42] etc. as means to enhance the conductivity of polyIL based systems.

In a series of studies, we have used atomistic simulations to examine the mechanisms underlying ionic conductivity in a variety of polyIL based systems.[33,43–49] In this context, our most recent study considered the ion mobilities and transport mechanisms in salt-doped polyILs.[50] Earlier work on salt-doped *neutral* SPEs such as polyethylene oxide had demonstrated that the ion motion in salt-doped systems is accomplished by the polymer segmental motion-assisted hopping between active sites on the polymer electrolytes.[51–56] Consequently, ion mobilities in such systems were coupled with the polymer segmental dynamics, or equivalently, the glass transition temperature of the system. In contrast to such findings for neutral SPE systems, our simulation work on lithium salt-doped poly(1-butyl-3-methyl-imidazolium bistrflimide), a polycationic IL, showed that lithium ion mobilities exhibited stronger dependence on polymer segmental dynamics in comparison to the anion mobilities.[50] Such simulation results qualitatively mirrored the experimental observations[41] on the influence of lithium salt concentration c_{Li} (the ratio of number of lithium ions to the number of polycations mole ratio) on mobile ion mobilities. Our results were rationalized by demonstrating that: (i) The transport pathways of anions intrinsic to pure polyILs becomes interrupted by the salt induced polycation-anion-lithium co-coordinations. Further, the mobilities of the intrinsic anions and the co-coordinated anions compensate each other, resulting in a "decoupled" dependence of anion dynamics on polymer segmental dynamics; (ii) The lithium ions were found to be indirectly coordinated to a number of polymer chains through the polycation-anion-lithium co-coordination, and thus, lithium ion mobilities exhibit a more "coupled" dependence on polymer segmental dynamics.

While the above study pertained to the regime of low salt concentrations ($c_{Li} \leq 0.4$), interesting experimental observations have also been reported at higher salt concentrations in such systems. Specifically, Wang *et al.* reported that the lithium mobilities become greater than the anion mobilities for $c_{Li} \gtrsim 1.0$.[41] Other related experiments have shown that the glass transition temperatures of the salt-doped polyILs increases at low salt concentrations and then plateaus at large c_{Li}.[34] Together, such observations are especially of interest, since they indicate that at higher salt concentrations, the transference numbers (i.e., the current carried by lithium relative to the total carried by lithium and anion) may increase without a concomitant decrease in the mechanical strength arising from the T_g reduction.

Motivated by the above experimental observations, in this study, we extended our atomistic molecular dynamics simulations on lithium salt-doped poly(1-butyl-3-methyl-imidazolium bistrflimide) to probe the mobilities and mechanisms of ion transport in the higher lithium salt concentration ranges (from $c_{Li} = 0.6$–1.8). Our results indicate that the polymer chain segmental dynamics plateaues at the high c_{Li} range due to a saturation of the co-coordination of polycations. While anion mobilities exhibit physics similar to that noted at low salt concentrations, the lithium ion mobilities become decoupled from the polymer chain segmental dynamics at higher salt concentrations due to a reduction in the number of ions coordinated with the polymer backbone. Together, our results help explain the mechanisms underlying the experimental observations for larger salt concentrations.

The rest of this paper is organized as follows: in the *computational methods* section we describe the setup of lithium salt-doped polyIL at high c_{Li} range, and the details of the different simulation quantification measures. In the *results and discussions* section we discuss the results of mobile ion diffusion coefficients, influence of c_{Li} on the polymer segmental dynamics, anion transport mechanisms and the lithium transport mechanisms. We conclude with a brief summary of our findings and conclusions in the *conclusions* section.

2 | COMPUTATIONAL METHODS

2.1 | Simulation details

In the present study, we used atomistic molecular dynamics simulations to investigate the structural and dynamical properties of poly(1-butyl-3-methyl-imidazolium bistriflimide) with added lithium salt. The setup of the simulated systems are listed in Table 1. Through the range of c_{Li}s, the number of polymer chains was fixed to 20, and the length of a single polymer chain was maintained at 15 monomer units.[44]

TABLE 1 Simulation details for different lithium ion concentrations c_{Li}. The length of a single polymeric ionic liquid chain is fixed at 15

Species	polyBmIm	TFSI	Lithium
$c_{Li} = 0.6$	20	480	180
$c_{Li} = 0.9$	20	570	270
$c_{Li} = 1.2$	20	660	360
$c_{Li} = 1.5$	20	750	450
$c_{Li} = 1.8$	20	840	540

The initial conformation of the single polymer chain was generated by using a multiscale simulation procedure.[57] In this procedure, a coarse-grained model of the polymer chain was equilibrated, and then the atomistic details of each coarse-grained bead were introduced through a reverse mapping approach based on the adaptive resolution scheme method.[58–60] A more detailed description of the multiscale simulation strategy could be found in our recent studies.[46,61]

The MD simulations were performed in Gromacs ver 2018.4.[62] The all-atom optimized potential for liquid simulations (OPLS-AA) was chosen for modeling the bond, angle, dihedral, improper torsions, and nonbonded interactions, as described in the following potential energy function:

$$U(r) = U^{bond}(r) + U^{angle}(\theta) + U^{dihedral}(\phi) + U^{improper}(\psi) + U^{nb}(r) \quad (1)$$

In Equation 1, the first two terms were modeled using the harmonic function form, the dihedral potential adopted the Ryckaert-Bellemans function form, the improper torsion employed the periodical function form and the nonbonded interactions could be written as[63]:

$$U^{nb}(r) = \sum_{i}^{N}\sum_{j>i}^{N} f_{ij}\left[4\epsilon_{ij}\left[\left(\frac{\sigma_{ij}}{r_{ij}}\right)^{12} - \left(\frac{\sigma_{ij}}{r_{ij}}\right)^{6}\right] + \frac{q_i q_j e^2}{r_{ij}^2}\right] \quad (2)$$

In Equation 2, f_{ij} was used to scale 1–4 interactions particularly by a factor of 0.5, the interactions beyond 1–4 interactions were not influenced and f_{ij} was set to 1.0. The pairwise Lennard-Jones (LJ) parameters (ϵ and σ) were explicitly listed in our recent papers,[33,46,50] and the geometric combining rule was used for generating the LJ parameters for cross-terms. The partial charges of polyIL (represented by trimer under the consideration of computational cost) were optimized by B3LYP/6-311 g** theory[64–66] using Gaussian 09.[67] The restrained electrostatic potential (RESP) was post-processed through Multiwfn package.[68,69] The resulting partial charges were further scaled down by a factor of 0.8 for obtaining better agreement of dynamical properties with respect to experiments.[47–49,70,71]

Similar to our recent study,[50] the equilibrated salt-doped polyIL systems were constructed by packing 20 polymer chains randomly into the simulation box (initial box length was 8 nm) with corresponding number of anions and lithium ions. A multi-step pre-equilibration inspired by the 21-step decompression method proposed by Colina and coworkers, was used to decompress the initial simulation box to the experimental densities.[72,73] A single loop of the multi-step pre-equilibration contained three steps: (i) 0.1 ns NVT simulation at 1000 K, (ii) 0.1 ns NPT simulation at 600 K and 100 bar, and (iii), 0.1 ns NPT simulation at 600 K and 1 bar. In our study, such a loop was repeated for eight times. The configurations resulting from final configuration was used for the production run with NPT ensemble for 110 ns, and the last 100 ns trajectories were used for analyzing the statistical and dynamical properties.

The leap-frog algorithm was used as an integrator with the integration time-step $\delta t = 1$ fs. The cut-off for 12–6 Lennard-Jones potential was set to 1.3 nm, and the long-range electrostatic interactions were calculated with the particle mesh method.[74] The V-rescale thermostat[75] was used for temperature coupling at 600 K and Parrinello-Rahman barostat[76] was used for pressure control at 1 bar, with the corresponding coupling parameters $\tau_T = 1.0$ ps and $\tau_P = 1.0$ ps. Ten samples with completely different initial configurations were used for averaging the presented statistical and dynamical properties.

2.2 | Ion coordination characteristics

The structural characteristics of polyIL systems were quantified by calculating the ion pair radial distribution function using

$$g_{ij}(r) = \frac{V}{N_i N_j}\left\langle \sum_{i}^{N_i}\sum_{j}^{N_j} \frac{\delta(r_{ij} - r)}{4\pi r^2} \right\rangle \quad (3)$$

where N_i and N_j are the number of atoms of ion species i and j. V is the time averaged volume of simulation box, and δ is the Dirac delta function. For the polycation $BmIm^+$, we chose the nitrogen atom that was connected to the butyl group to represent the reference, and for the anion TFSI, we also used the nitrogen atom as the reference. Further, many of the statistical properties presented in later sections, such as the anion-polycation coordination and lithium-anion coordination, were calculated based on the cutoff of different ion pairs. The cutoff was determined by the position r where $g(r) = 1.0$ after the first peak.

2.3 | Transport properties

To quantify the transport properties, we used the mean square displacements (MSDs) to derive the diffusion coefficients of the mobile TFSI anion and the lithium cation species. For the anion TFSI, instead of using the center of

mass of the entire molecule, we used the nitrogen atom to represent the reference for calculating the MSD. The diffusion coefficient D was calculated by using the Einstein relation

$$D = \lim_{t\to+\infty} \frac{1}{6t} \left\langle (\boldsymbol{r}(t) - \boldsymbol{r}(0))^2 \right\rangle \tag{4}$$

where $\boldsymbol{r}$ is the position vector of the corresponding atom of mobile ion species.

Another important transport property is the "ideal" transference number, which can be deduced based on the diffusivity:

$$t_{Li} = \frac{n_{Li} D_{Li}}{n_{Li} D_{Li} + n_{TFSI} D_{TFSI}} \tag{5}$$

In Equation 5, n_i denotes the number of ions of the type "i" ($i = Li, TFSI$). The contribution arising from the mobility of polycations was ignored, since we have demonstrated in our recent study that the diffusion coefficient of polycation was about two orders of magnitudes smaller in comparison to that of anion.[20]

2.4 | Polymer segmental dynamics

The segmental dynamics of the polyIL was probed through the auto-correlation function (ACF) of the dihedral angle of the polymer backbone. Since the backbone of poly(1-butyl-3-methyl-imidazolium bistriflimide) was polymerized from the polyethylene, so the entire backbone only has carbon atoms. Thus, the ACF of dihedral angle C—C—C—C was calculated as

$$C_{\Phi\Phi}(t) = \frac{\langle \cos\Phi(t)\cos\Phi(0)\rangle - \langle \cos\Phi(0)\rangle^2}{\langle \cos\Phi(0)\cos\Phi(0)\rangle - \langle \cos\Phi(0)\rangle^2} \tag{6}$$

where $\Phi(t)$ is the dihedral angle at time t and $\Phi(0)$ is the dihedral angle at the reference time. We fit $C_{\Phi\Phi}(t)$ to a stretched exponential of the form,

$$C_{\Phi\Phi}(t) = \exp\left(-\left(\frac{t}{\alpha}\right)^{\beta}\right) \tag{7}$$

and calculated the relaxation timescale $\tau_{\Phi\Phi}$ of the segmental dynamics by the following equation

$$\tau_{\Phi\Phi} = \alpha\Gamma\left(1 + \frac{1}{\beta}\right) \tag{8}$$

where Γ denotes the Gamma function.

3 | RESULTS AND DISCUSSIONS

3.1 | Ion diffusion coefficients

We first discuss the results for the diffusion coefficient of different ion species. In Figure 1A, we display the results for the mobile ion species TFSI and lithium. In accord with the results presented in our recent study,[50] the diffusivity of all mobile ion species increase with increasing lithium salt concentration c_{Li} in the range from 0.0 to 0.4. Further, the anion diffusivities are observed to be much less sensitive to c_{Li} in comparison to those of lithium ions. For salt concentrations $c_{Li} > 0.4$, the anion mobilities are however observed to approach a plateau. In

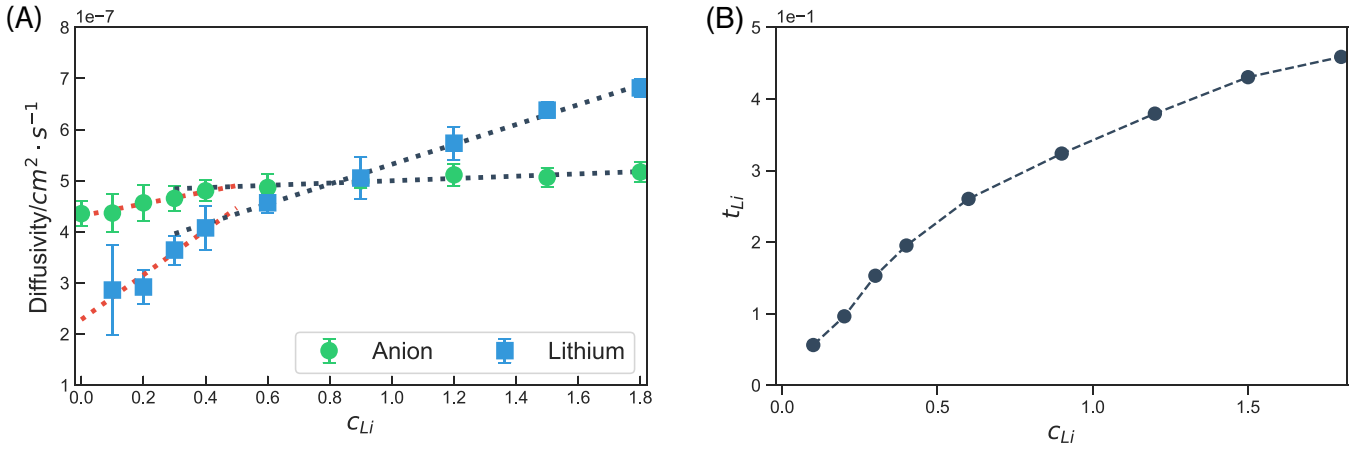

FIGURE 1 (A) Diffusion coefficients of anions and lithium as a function of lithium concentration c_{Li}. The dotted lines are a guide to the eye. The higher concentrations are shown through grey dotted lines and the lower salt concentrations are shown by red dotted lines (The raw MSDs and their fittings are shown in SI section S1); (B) The ideal transference number t_{Li}

contrast, the lithium mobilities are seen to increase with increasing c_{Li}, with however the mobilities becoming less sensitive to salt concentration. As a consequence of the different behaviors of the ion mobilities, the "ideal" transference number t_{Li} (cf. Equation 5) increases with increasing c_{Li}, as shown in Figure 1B.

We note that the above results qualitatively accord with the trends reported in earlier experimental results.[41] Explicitly, in the experiments, the diffusivity of lithium was observed to be less than that of anion in the low c_{Li} range, but became larger than that of anion in the high c_{Li} range. Furthermore, the anion mobilities were also observed to be less sensitive to c_{Li} in comparison with those of lithium ions. At even higher c_{Li} range, the diffusivity of both anion and lithium were found to decrease with increasing salt concentrations—a regime not captured within the c_{Li} probed in our study.[31,41]

In the experimental studies, the initial increases in ion mobilities at low salt concentrations were attributed to the decreased glass transition temperature T_g of the matrix. In our earlier computational study, we observed that such effects manifested in the polymer chain backbone dihedral relaxation timescale $\tau_{\Phi\Phi}$. Such changes in the polymer dynamics were rationalized by the reduction in the polycation-anion-lithium co-coordinations[41,50] occurring with increasing salt concentration.

In order to probe the physics accompanying higher salt concentrations, the polymer chain backbone dihedral relaxation timescale $\tau_{\Phi\Phi}$ was calculated and the results are shown in Figure 2. It can be seen that the inverse $\tau_{\Phi\Phi}$ increases at the low c_{Li} range, but seems to plateau beyond $c_{Li} = 0.4$. We note that such results also qualitatively agrees with the experimental results of T_g reported for higher salt concentrations.[41]

Along the lines of our previous study,[50] we examined the correlation between the ion diffusivities and polymer segmental relaxation times. In Figure 3, we display the anion and lithium diffusion coefficients as a function of $\tau_{\Phi\Phi}^{-1}$. It can be seen that the anion mobilities exhibits an identical dependence on the polymer segmental dynamics at higher salt concentrations as was noted for the low salt concentrations. In contrast, the lithium diffusion coefficients at higher salt concentrations seems to exhibit no correlation to the polymer chain segmental dynamics.

Together, the above results serve as the focal point of the issues we seek to address in the remain portion of this article. Explicitly, in the following section *polymer segmental dynamics*, we probe the origins of the modified dependence of polymer segmental dynamics on c_{Li} at higher salt concentrations. In section *anion transport mechanisms*, we present results probing the mechanisms of anion motion and establish the reasons underlying the plateauing seen in the mobilities at higher salt concentrations. In section *lithium transport mechanisms*, we present results probing the mechanisms of lithium-ion motion and the resulting impact on the correlation between lithium mobilities and polymer segmental dynamics.

3.2 | Polymer segmental dynamics

In our recent study at low c_{Li}, we demonstrated that with the addition of salt, the intrinsic polycation-anion-polycation coordinations are replaced by polycation-anion-lithium-anion-polycation co-coordinations.[50] In Figure 4 we show an illustration of such direct polycation coordination and the lithium mediated co-coordination. Therein, the original anion is seen to be coordinated with four polycations from two distinct polymer chains. However, after adding lithium salt, the polymer chains are indirectly linked through the co-coordinated anions.[41] We argued that the replacement

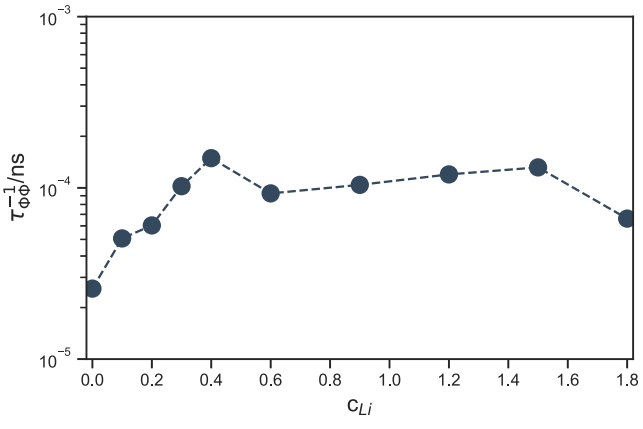

FIGURE 2 Dependence of inverse polymer chain backbone relaxation timescale $\tau_{\Phi\Phi}^{-1}$ on the lithium concentration c_{Li}

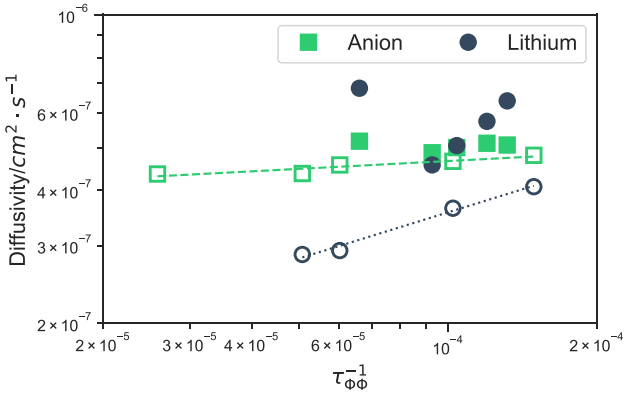

FIGURE 3 Dependence of mobile ion diffusion coefficient on $\tau_{\Phi\Phi}^{-1}$, the data points at low c_{Li} range (hollow markers) were reported in our recent study.[50]

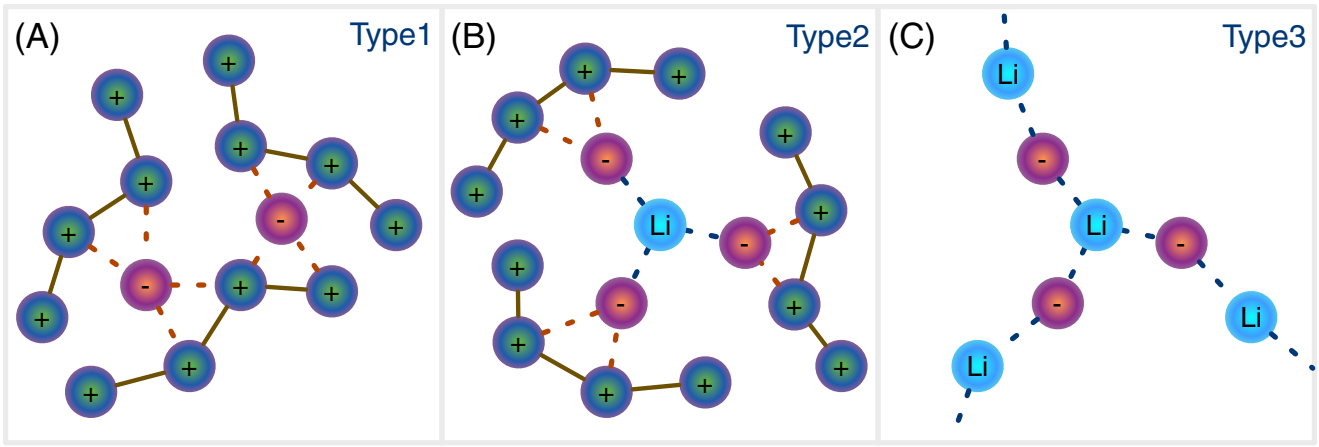

FIGURE 4 Illustration of: (A) Normally coordinated anion (Type1) that only associates with polycation; (B) Co-coordinated anion (Type2) that associates with both polycation and lithium; and (C) anions (Type3) that are only associated with lithium

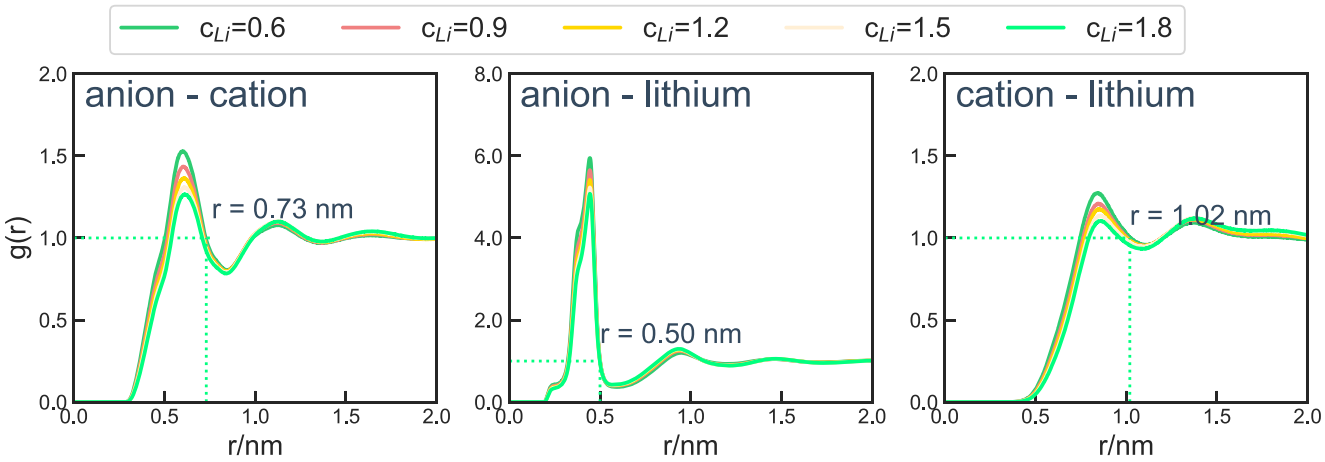

FIGURE 5 Radial distribution functions for TFSI (anion) and $BmIm^+$ (cation), TFSI and lithium, and $BmIm^+$ and lithium

of such direct polycation coordinations by the *weaker* lithium mediated co-coordination constituted the origin of the faster polymer dynamics.

To probe the influence of salt content on the ion pair interactions, the radial distribution function $g(r)$ for different ion pairs were calculated and the results are displayed in Figure 5. It can be seen that for all three ion pairs (TFSI (anion) and $BmIm^+$ (cation), TFSI and lithium, and $BmIm^+$ and lithium), increasing salt content leads to a decrease of the intensity of $g(r)$, indicating a reduction of the ion pair interactions. In comparing the three interactions, the intensity of $g(r)$ between anion and lithium is seen to be much higher than that of between anion and polycation, which suggests the preference for the anions to associate with the added lithium, thereby disrupting the existing polycation-anion-polycation coordination "bridges."

Next, we categorized the polycations themselves into two groups: (i) CT1: Polycations involved in coordination of the form polycation-anion-polycation; and (ii) CT2: Polycations that are involved in the co-coordination form of polycation-anion-lithium. In Figure 6 we show the results for the polycation coordination statistics as a function of salt concentration. We can see that at the low c_{Li} range (<0.6), the fraction of CT1 polycations decreases monotonically and the fraction of CT2 polycations increases monotonically. However, at high c_{Li} range, more that 90% of the polycations are seen to participate in co-coordination with lithium, and that there is no further change in the coordination behavior of cations. This behavior can be understood by noting that there are a fixed number of polycations in the system, which prevents further increase in the co-coordination with the added lithium.

The results of Figure 6 can be used to rationalize the dependence of polymer segmental dynamics on the salt concentration. More explicitly, the acceleration of polymer dynamics seen at low salt concentrations arises from

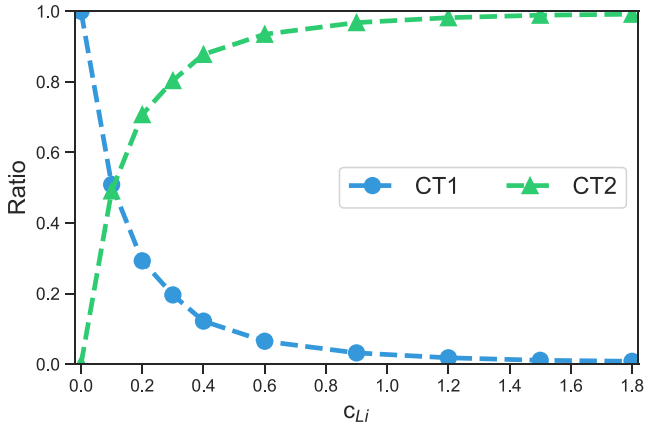

FIGURE 6 Fraction of different polycation coordination types, CT1 indicates polycations that are only associated with the anions and CT2 represents polycations that are indirectly associated with lithium through the Type2 anion

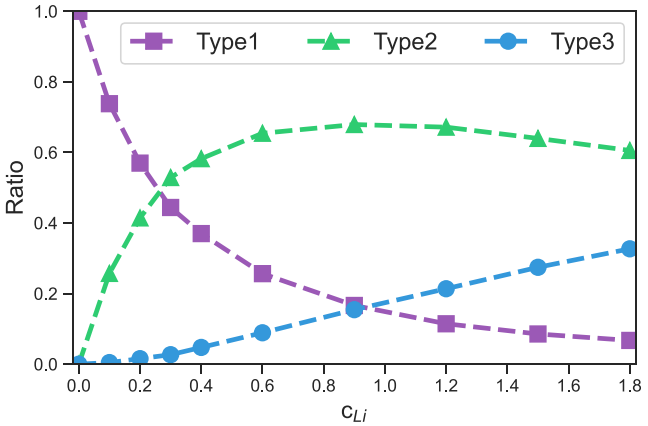

FIGURE 7 Fraction of different TFSI coordination types

the decrease in CT1 (the intrinsic polycation-anion-polycation coordination) and the accompanying increase in the co-coordinated CT2 cations. However, the saturation of CT1 and CT2 seen at higher salt concentrations leads to a plateauing of the effect of co-coordinations and its impact on polymer segmental dynamics.

3.3 | Anion transport mechanisms

In our previous study at low salt concentrations,[50] we rationalized the results for anion mobilities by considering the dynamical characteristics individually of the anions involved in CT1 and CT2 coordinations. Such anions were termed respectively as Type1 and Type2 anions. The Type1 ions were seen to retain the structural characteristics exhibited by anions in pure polyILs (i.e., in the absence of salt),[43] and were coordinated with four cations from two different polymer chains. In contrast, Type2 anions exhibited modified coordination characteristics involving one polymer chain and fewer cations. More importantly, the Type1 anions maintained their identity during their motion—that is, a Type1 anion was most likely to transform to a Type1 anion during a hop and maintain its coordination characteristics. However, in the presence of Li salt, such pathways were hindered due to the existence of Type2 anions exhibiting distinct coordination characteristics. Hence, the dynamics of the Type1 anions became slower with increased salt concentrations. In contrast, since the Type2 ions requires only one polymer chain for its coordination and hopping, their pathways were much less impacted by the presence of Type1 ions. Further, since such anions were coupled to a single polymer chain, their dynamics was faster than Type1 anions. Together, the overall mobility of the anions was rationalized as a "compensation" effect between the slower dynamics of Type1 ions and the faster dynamics (and increasing populations) of Type2 ions.

To understand the anion transport mechanisms underlying the results of Figure 1 for higher salt concentrations, anion coordination in salt-doped polyIL systems were categorized into three groups[50]: (1) Type1 anions that are associated only with polycations; (2) Type2 anions that are associated with both polycation and lithium through the co-coordination (polycation-anion-lithium); and (3) Type3 anions that are only associated with lithium.

The fractions of the three types of coordinated anions are shown in Figure 7. It can be seen that the fraction of Type1 anion decreases with increasing c_{Li}, confirming the reduction in the intrinsic polycation-anion-polycation "bridges." The fraction of Type2 (co-coordinated) anion is seen to increase for low c_{Li} range and decreases at higher salt concentrations. The latter behavior can be rationalized by the fixed number of polycations in the system which prevents a monotonic increase in the co-coordination (akin to the saturation effect seen in the polycations CT2). The fraction of Type3 anion is seen to increase monotonically with salt concentration. We recall the fractions of the three types of coordinated anions in our recent study[50] that at low c_{Li} the contribution of fraction of Type3 anion was negligible. In contrast, at high c_{Li} range, we observe that the fraction of Type3 anions are significant and even higher than that of Type1 anions after $c_{Li} > 0.9$.

We further characterized the coordinations of the anions with the polycation by using the anion pair probability distribution, $P(n)$, that a given anion is associated n polycations (Figure 8). It is observed that $P(n)$ exhibits comparable peaks at $n = 3$ and $n = 2$ when $c_{Li} = 0.6$, and the peak moves towards to smaller n with increasing c_{Li}.

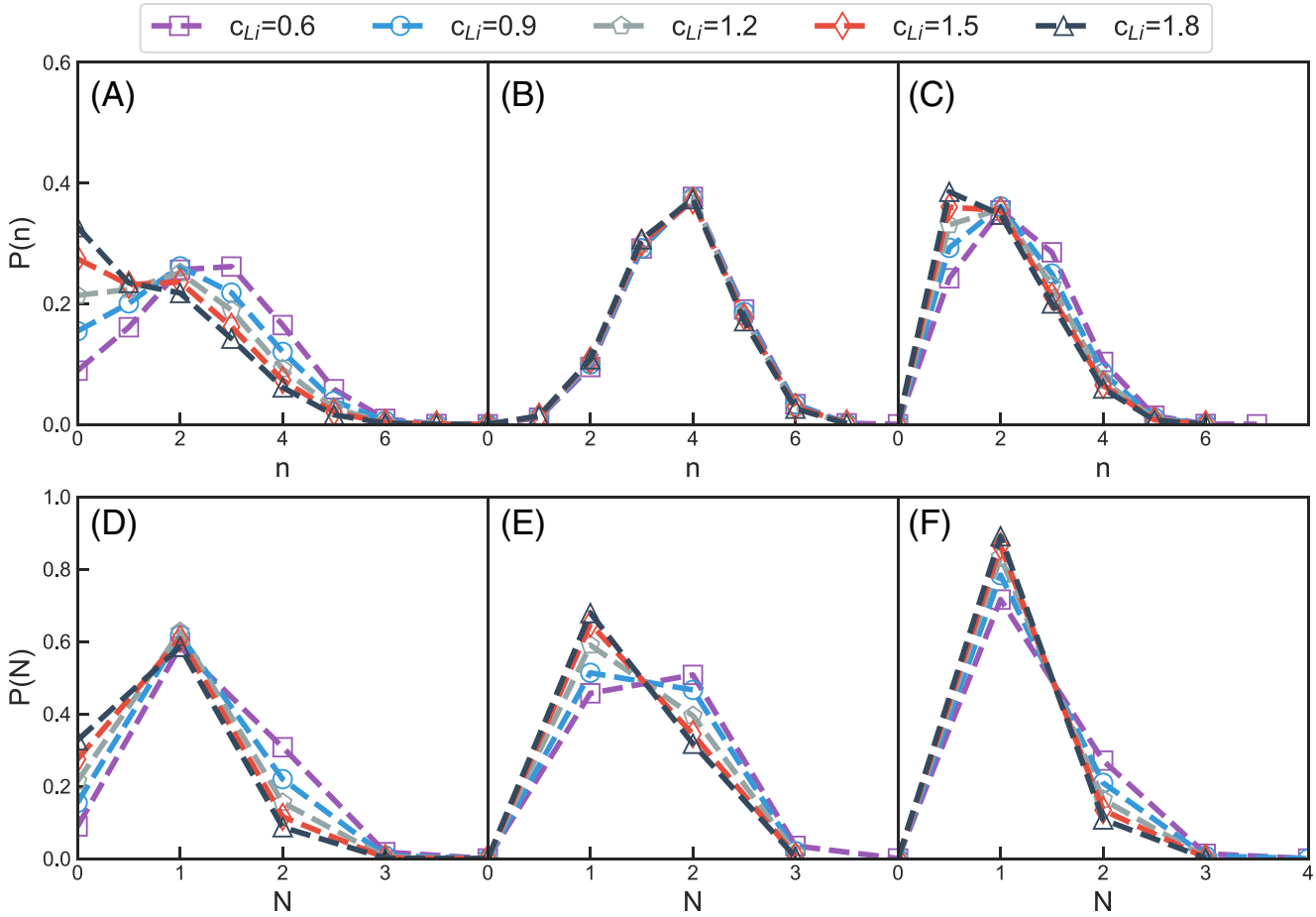

FIGURE 8 Probability that a given TFSI is associated with n polycations: (A) The overall anions; (B) Type1 anions; and (C) Type2 anions. Probability that a given TFSI is associated with N polymer chains: (D) The overall anions; (E) Type1 anions; and (F) Type2 anions

At the same time, the probability $P(n)$ for $n = 0$, where the given anion doesn't associate with any polycations increases with salt concentration, which is in consistent with the trend of the fraction of Type3 anions in Figure 7.

We decompose the overall anion pair probability distribution (Figure 8A) into the $P(n)$s for subgroups Type1 and Type2 anions respectively in Figure 8B, C. It can be seen in Figure 8B that the lithium salt concentration c_{Li} doesn't influence the coordination characteristics $P(n)$ of Type1 anions. In contrast, as shown in Figure 8C, for Type 2 anions, the probability distribution $P(n)$ displays peaks at $n = 1$ and $n = 2$.

Next, in Figure 8D–F we turn to the influence of lithium salt content on the probability distribution that a given anion is associated with N distinct polymer chains, $P(N)$. At low c_{Li} range,[50] our earlier study showed that $P(N)$ displays a peak at $N = 2$, corresponding to an association with two polymer chains. In contrast, at higher salt concentrations probed in this study, the overall $P(N)$ is seen to display a sharp peak at $N = 1$ and accompanies an increased probability at $N = 0$.

The decomposition of $P(N)$ into subgroups for Type1 and Type2 anions are shown in Figure 8E,F. Explicitly, the $P(N)$ of Type1 anions shows comparable peaks at $N = 2$ and $N = 1$ when $c_{Li} = 0.6$, and the peak moves towards $N = 1$ with increasing c_{Li}. In contrast, the $P(N)$ of Type2 anions displays a extremely sharp peak at $N = 1$, and the probability is above 0.7 for all investigated c_{Li}s.

Next, we present the results of lithium coordination characteristics of Type2 and Type3 anions in Figure 9. We can see from Figure 9 that the lithium coordination increases with increasing c_{Li} for both Type2 and Type3 anions, suggesting the formation of larger anion-counterion complexes at higher salt concentrations.

Finally, in Figure 10 we present a frame analysis of the hopping motion and the probabilities of interconversion (if any) between the different types of anions during such a motion (the hopping motion is defined by checking the identity of a given anion between t_0 and $t_0 + \Delta t$. For example, a given anion at t_0 is Type1, after Δt ($\Delta t = 1$ ps), if the given anion still maintains its original identity, then it is still counted as *Type1*; if its identity changes to Type2, then it is counted as *Switch Type1*→

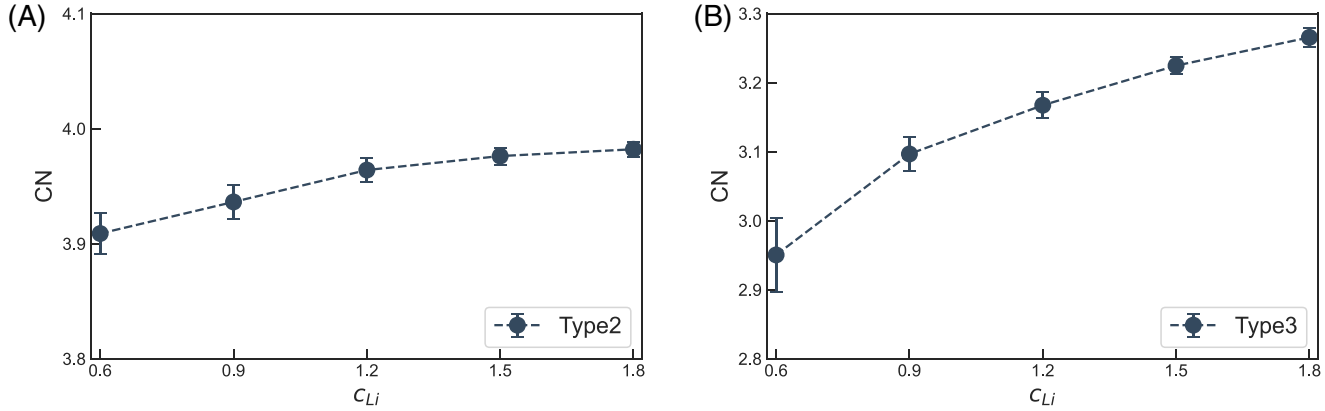

FIGURE 9 The coordination number (CN) at the first solvation shell for (A) Type2 and (B) Type3 anions as a function of lithium salt concentration c_{Li}

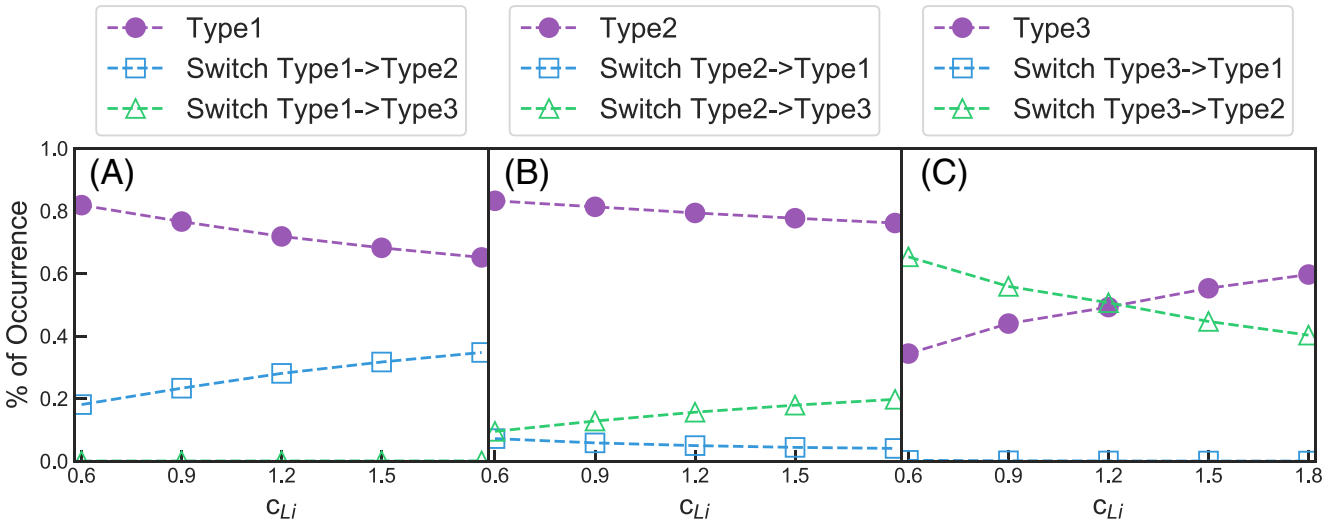

FIGURE 10 Probability of hopping events for (A) Type1 anions, (B) Type2 anions and (C) Type3 anions. The solid (open) symbols pertain to the probability that a given anion retains (changes) its identity after hopping

Type2; if its identity changes to Type3, then it is counted as *Switch Type1→Type3*, a more detailed description of the methodology can be found in our recent study.[50]). Despite the fact that the coordination characteristics of Type1 anions are modified relative to pure polyIL, we see from Figure 10A that a majority of Type1 anions still maintain their identity after the occurrence of a hopping event occurs. However, with increasing c_{Li}, there is an increase in the probability of Type1 anions switching to Type2 anions. As shown in Figure 10B, the Type2 anions are also seen to have a high probability to retain their identities after hopping events, although such probability decreases slightly as a function of c_{Li}. Different from Type1 and Type2 anions, it is seen from Figure 10C that the Type3 anions initially exhibit a greater propensity to switch to Type2 anions. At higher salt concentrations, we observe that the motion of Type3 anions becomes more towards retaining their identity. Surprisingly, the occurrence rate for Type1 anions switching to Type3 anions (and *vice versa*) is negligible (almost zero), indicating an intermediate step is necessary for converting the identity from Type1 anions to Type3 anions (or from Type3 to Type1 anions).

The above results shed light on some of the factors influencing the transport of Type1 anions. It was observed (Figure 7) that at higher salt concentrations, Type2 and Type3 anions become the dominant modes of coordination. As a result of the distinct coordination characteristics of Type2 and Type3 anions, Type1 anions exhibit coordination different from those in pure polyIL, and are mostly coordinated with a single polymer chain. Such modified coordination is expected to impact the transport pathways of Type1 anions (which involve intramolecular hopping along two polymer chains while coordinated with four polycations[33,43–46,61]). Consistent with

such an expectation, at higher c_{Li}, there was an increase in the probabilities of hopping events leading to a switch of Type1 to Type2 anions. Together, we expect that due to these factors, the mobilities of the Type 1 anions to become reduced with increasing salt concentration.

With regard to Type2 and Type3 anions, the mobilities of such ions are expected to be inherently faster than that of Type1 anions since they are coordinated with only one polymer backbone (as deduced from the $P(N)$) and hence can move faster than Type1 anions. However, in Figure 9, we observed an increased anion-lithium coordination at higher salt concentrations. In the context of mixtures of salt and pure ionic liquids,[77,78] such increased anion-lithium clustering has been shown to lead to a reduction in the mobility of the anions. Hence, we may expect a similar phenomena to manifest in our system and lead to a slowing of the Type2 and Type3 anions with increasing salt concentration.

In Figure 11, we present short time MSDs for Type1, Type2 and Type3 anions to validate the hypotheses advanced above. In Figure 11A, it can be seen that the mobilities of Type1 anions are indeed slower than those for pure polyILs. Moreover, with increasing salt concentrations, it can be observed that there is a further reduction in the mobilities of Type1 anions. With respect to Type2 and Type3 anions, it can be seen that the inherent mobilities are higher than that of Type1 anions (and those in pure polyIL). However, with increasing salt concentrations, it can be seen that there is a reduction in their mobilities arising from the increased coordination with the lithium ions.

The compensation of the mobilities of the three types of anions (weighted by their respective fractions) is shown in Figure 11D. Due to the hierarchy of the mobilities of the different types of anions, their fractions, and the dependence on the salt concentration, we observe that the net mobility of the anions are almost independent of the salt concentration. Together, such results rationalize the results for the anion mobilities observed in Figure 1.

3.4 | Lithium transport mechanisms

In our recent study for low salt concentrations,[50] we showed that the majority of the lithium ions are associated with the co-coordinated anions (Type 2). Moreover,

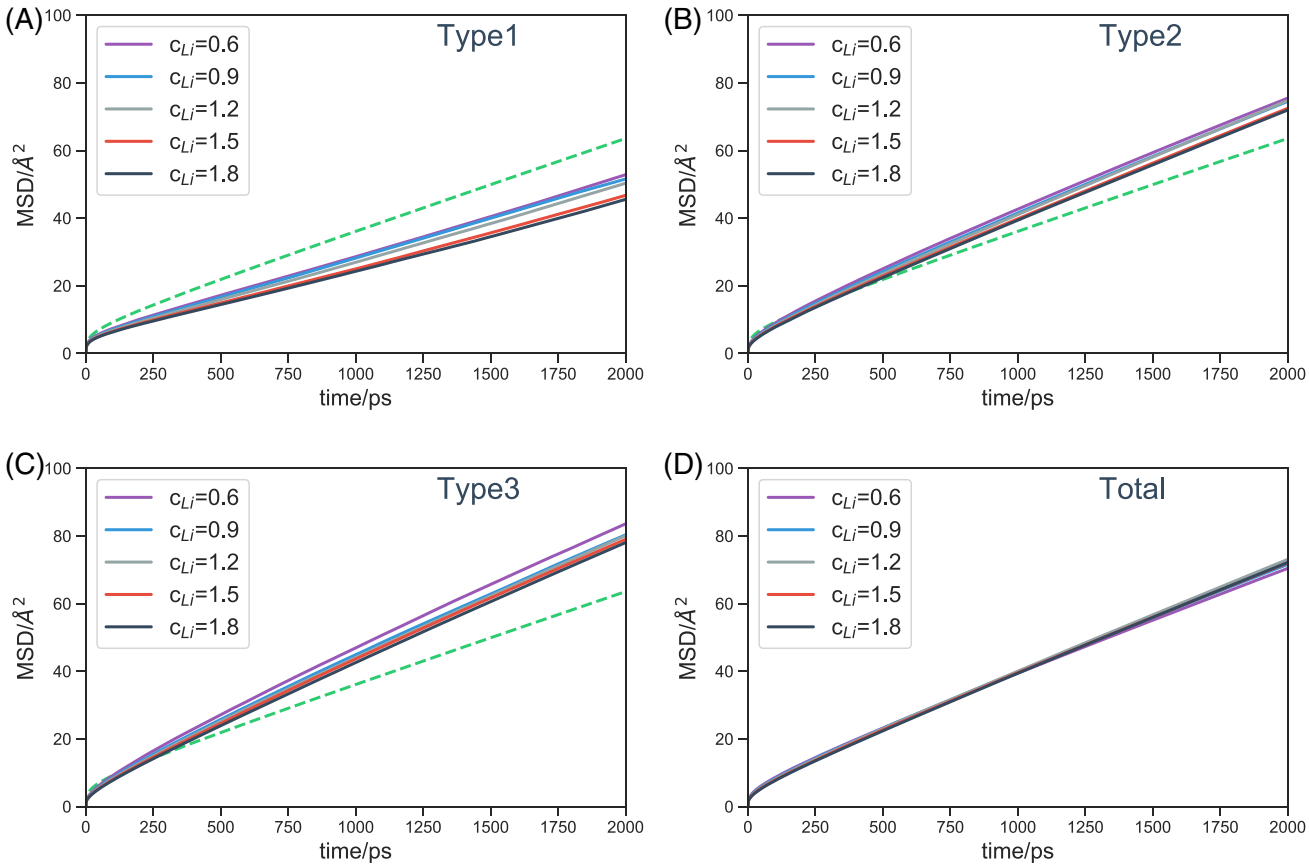

FIGURE 11 The short time mean square displacements for: (A) Type1 anions; (B) Type2 anions; (C) Type 3 anions; (D) All anions. The results for $c_{Li} = 0.0$ is displayed as a benchmark

such lithium ions were shown to be involved in a big cluster of coordination surrounded by about six polycations and five to ten polymer chains. Such observations were used to rationalize the coupling lithium mobilities to the polymer chain segmental dynamics. For the higher salt concentrations examined in this study, we observed in Figure 1 that the lithium diffusivities increases with c_{Li} despite an almost constant polymer dynamics. In this section, we present results examining the origins underlying such trends considered within the context of the mechanisms of lithium ion motion.

First, we consider the mechanism of lithium ion transport in salt-doped polyIL systems. In general, lithium ion motion in such systems have been suggested to be of two broad kinds, namely the *vehicular* motion where the given lithium moves with its first coordination shell, and the *structural* diffusion where the anion identities that are surrounding the given lithium ion are refreshed after the hopping. In our recent study, we used a method of analysis which relied on monitoring ion association/dissociation hopping events between neighboring frames.[61] Based on such analysis we concluded that (at low salt concentrations), lithium ions primarily move by the vehicular mechanism involving the first coordination shell of anions. In the SI Section S2, we show the results for lithium hopping events based on neighboring frame analysis at higher concentration regimes, which again indicates a vehicular motion dominated transport mechanism.

However, analysis based on neighboring frames suffers from the drawback that association/dissociation events that go back and forth (rattling) are counted as unique hopping events, and can lead to erroneous conclusions.[79] As a means to overcome such issues, in this work we adopted a different procedure based on the status of the lithium solvation shell and its persistence during the motion of the lithium ions. Towards such an objective, we use the continuous lithium solvation shell autocorrelation function, $S(t)$, to characterize the average lifetime of the solvation shell:

$$S(t) = \langle h(t_0) \cdot H(t_0 + t) \rangle \tag{9}$$

where $h(t_0)$ equals one indicating initial association status of an existing lithium solvation shell, and $H(t)$ is given as:

$$H(t') = \begin{cases} 1, & (h(t) = 1) \forall (t_0 \le t' < t_0 + t) \\ 0, & otherwise \end{cases} \tag{10}$$

such that $H(t)$ equals one only if the initial association status of the lithium solvation shell keeps the same continuously between time t_0 and t and zero otherwise. To quantify the persistence of the lithium solvation shell, the autocorrelation function $S(t)$ was fitted to a stretched exponential form:

$$S(t) = \exp\left(-\left(\frac{t}{\alpha}\right)^{\beta}\right) \tag{11}$$

and the characteristic timescales were evaluated as:

$$\tau_{Solvation} = \alpha \Gamma\left(1 + \frac{1}{\beta}\right) \tag{12}$$

The fitted $\tau_{Solvation}$ is displayed in Figure 12A, where it can be observed that the average lifetime of lithium solvation shell decreases with increasing c_{Li}, indicating that the lithium solvation shell becomes more and more unstable with increasing salt concentration. Such results hint that that vehicular motion is not the likely mechanism of ion transport in such systems (the lithium solvation shell autocorrelation function $S(t)$ is shown in SI Section S3), and that the contribution of structural diffusion may increase with increasing c_{Li}.

To further quantify the contributions of vehicular motion and structural diffusion to the overall lithium transport events, we calculated the probability distribution of lithium travel length before the solvation shell is renewed. It can be seen from Figure 12B that the probability distributions of lithium travel length are quite similar throughout the c_{Li} we investigated, with a peak around 1.2 Å. A slight increase in peak intensity with c_{Li} can be observed. The latter is consistent with the results of $\tau_{Solvation}$ due to the shorter distance the lithium could travel with decreasing lifetime of solvation shell. More directly, we show the average travel length in Figure 12C, where one can see a decreasing trend as the c_{Li} increases.

At a practical level, the size of the counterion on the solvation shell (2 times the radius of gyration R_g) is used as the probe to distinguish whether the transport event of the given ion belongs to the vehicular motion or structural diffusion. In the present study, the radius of gyration R_g of anion TFSI is measured as 2.5 Å at 600 K (it has been reported in the literature that the size of anion TFSI is about 2.6 Å at 400 K[80]). If the travel length of a given lithium is larger than the size of counterion before the solvation shell is refreshed, this lithium can be counted as undergoing a vehicular motion event, otherwise, the lithium will be counted as undergoing a structural diffusion event. From the results displayed in Figure 12B, we observe that the probability distribution of lithium travel length is approximately zero when the travel length is close to 5.0 Å, indicating almost none of the lithium travels a distance of the anion size before the solvation shell dies.

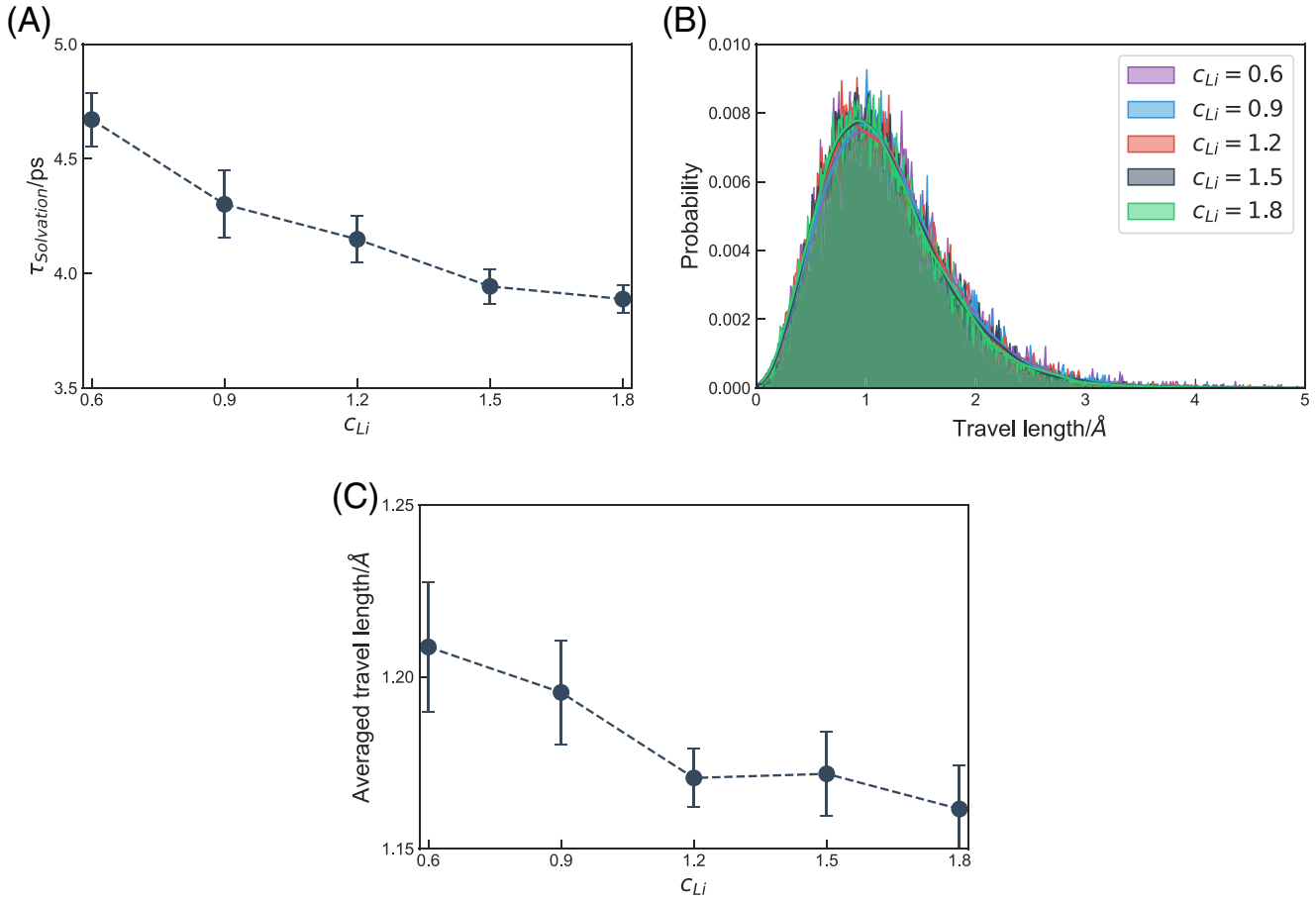

FIGURE 12 (A) The lithium solvation shell lifetime $\tau_{Solvation}$ as a function of lithium concentration c_{Li}; (B) The probability distribution of lithium travel length before its first solvation shell died; and (C) The average travel length of lithium before the first solvation shell died

Together, the above analysis based on the lifetime of lithium solvation shell demonstrates that the lifetime of the lithium solvation shell is too short to facilitate a vehicular motion of the lithium ions in our system. Instead, the lithium ions primarily moves by a structural diffusion mechanism in which there is a renewal of the solvation shell facilitated by the hopping of the lithium ions. With such a background, below we analyze the coordination characteristics of the lithium ions to understand the origins of the mobility increases with increasing salt concentrations seen in Figure 1.

Similar to the classification of polycation and anion types, the lithium ions were also categorized into different subgroups characterizing their coordinations respectively with Type2 anions and Type3 anions. Lithium ions which are co-coordinated with Type2 anions and polycations are denoted as LT1, and the lithium ions which are only associated with Type3 anions are denoted as LT2. As seen in the results displayed in Figure 13, the fraction of lithium ions (LT1) associated with Type2 anions decreases with increasing c_{Li}. Correspondingly, the fraction of lithium ions associated with the Type3 anions (LT2) are seen to increase monotonically. However, more importantly, in the concentration range probed in the present study, we observe almost 85% of the lithium ions are still co-coordinated (i.e., of the type LT1), suggesting that a closer consideration of the dynamics of such ions may serve to explain the results observed in the lithium ion mobilities.

In Figure 14A we display the probability distribution $P^{LC}(n)$ that a given lithium ion of LT1 kind is associated with n polycations through co-coordination (polycation-anion-lithium). With increasing salt concentration, the peak in $P^{LC}(n)$ is seen to move from $n = 5$ to $n = 2$, demonstrating a reduction in the number of polymers coordinated with the lithium ion. The reduction of constraints on the lithium ions can be further confirmed by the probability distribution $P^{LP}(N)$, which quantifies the probability that a given lithium ion is indirectly associated with N distinct polymer chains, as shown in Figure 14B. We can see that with increasing salt concentrations, the peak shifts from $N = 5$ to $N = 2$, suggesting a decrease in the size of the co-coordination cluster involving lithium and the polycations.

To summarize, the results presented in Figures 12 and 13 demonstrate that: (a) The lithium ions move primarily

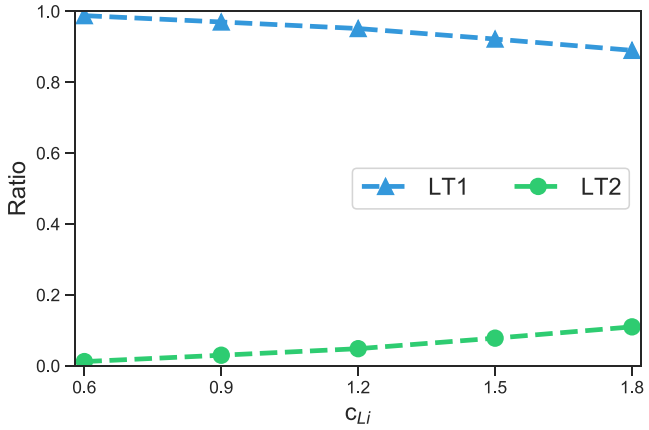

FIGURE 13 Fraction of different lithium coordination types, LT1, lithium ions that are co-coordinated with Type2 anions and polycations, and LT2, lithium ions that are only associated with Type3 anions

by a structural diffusion involving a refreshing of the solvation shell; (b) For the majority of the lithium ions, the solvation shell is comprised of co-coordination Type2 anions; (c) The number of polycations and the unique polymer chains involved in such coordination decreases with increasing salt concentration. Based on such observations, we can hypothesize that the constraints (i.e., the solvation shell which needs to be refreshed) becomes weaker with increasing salt concentration, facilitating the faster lithium ion motion.

While a partial confirmation of the above hypothesis was seen in the lifetime of the solvation shell (we note that the solvation shell considered for the results in Figure 12 included both LT1 and LT2 ions), in order to prove more conclusively that the LT1 lithium ions are indeed less constrained, the short time MSDs for LT1 and LT2 lithium ions are shown in Figure 15. It is observed that

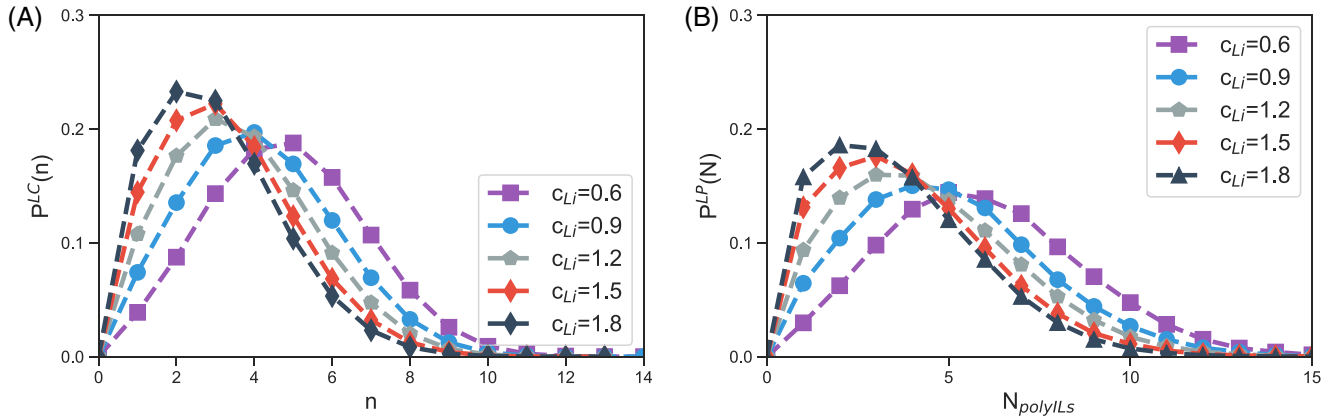

FIGURE 14 (A) Probability $P^{LC}(n)$ that a give Li is associated with n polycations through the Li-anion-polycation co-coordination; and (b) probability $P^{LP}(n)$ that a give Li is associated with N polymer chains. (the probability $P^{LA}(n)$ that a give Li is associated with n anions and the corresponding coordination number (CN) are shown in SI Section S4)

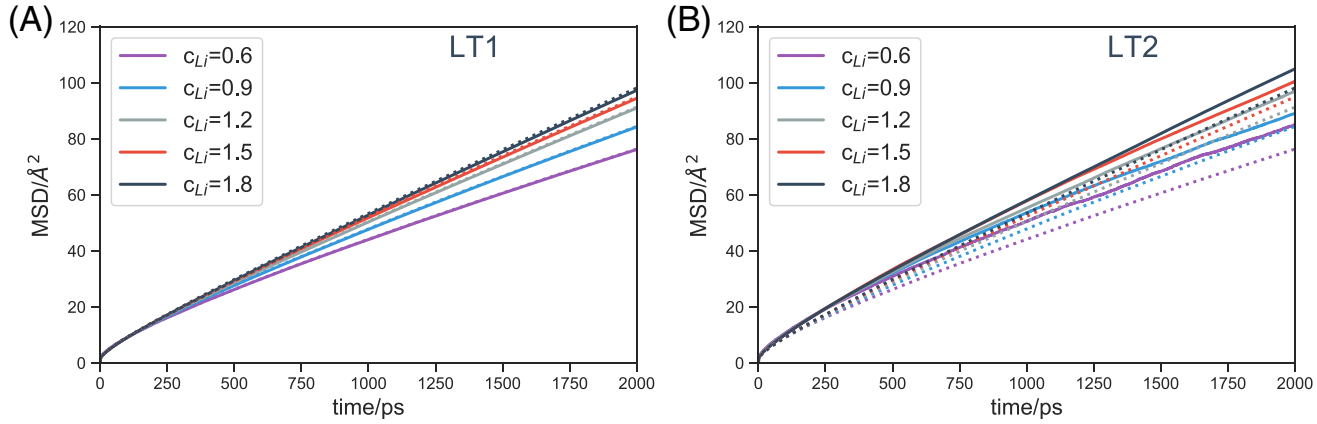

FIGURE 15 The short time mean square displacements for: (A) Lithium type LT1; (B) Lithium type LT2. The dotted lines are the overall short time mean square displacements (MSDs) and displayed as a benchmark

the mobilities of both types of lithium ions increase with increasing c_{Li}. When considered in conjunction with the fraction of LT1 lithium ions constituting the majority of the lithium ions, the results of short time MSDs demonstrate that the reduced constraints on the lithium ions facilitate the faster lithium ion mobilities seen in Figure 1A.

4 | CONCLUSIONS

In this work, we used atomistic simulations to study the mechanisms of ion transport in salt-doped polymeric ionic liquid systems at higher salt concentrations. Consistent with related experimental observations, our simulations indicated that at higher salt concentrations, the anion mobilities become lower than that of the lithium cations. Further, the anion mobilities became relatively insensitive to that the salt concentration while the mobilities of lithium increased with increasing salt concentration.

We rationalized the result for the anion mobilities by considering the fractions of anions which are exclusively coordinated with the polycations (Type1), co-coordinated with cations and lithium (Type2) and exclusively with lithium (Type3). By considering the coordination characteristics of the different types of anions and their hopping motions, we demonstrated that the net anion mobilities results from a compensation effect of the hierarchy and the salt concentration dependence of the different anions.

With respect to the lithium ions, we demonstrated that the lithium ions move primarily by a structural diffusion involving a refreshing of the solvation shell. Further, for the majority of the lithium ions, the solvation shell was comprised of co-coordination Type2 anions, and that the number of polycations and the unique polymer chains involved in such coordination decreases with increasing salt concentration. Such changes were shown to weaken the solvation shell around the lithium, thereby facilitating faster ion motion.

A key objective of SPEs is to be able to achieve high transference numbers without a concomitant reduction in the mechanical strength. Our results suggest that a possible means to achieve this in salt-doped polyILs is to use anions which exhibit a stronger coordination to the polycation in comparison to that of the lithium. Through such means, the strength of the solvation shell around lithium is expected to be weakened, facilitating faster lithium ion motion. In contrast, the anion coordination with the polycation is expected to be enhanced, resulting in slower anion motion. Further, since the lithium co-coordination tendencies are expected to be weakened, the segmental dynamics (and the mechanical strength) is expected to be less influenced by the added salt.

ACKNOWLEDGMENTS

The authors work on the topic of ion transport in polymer electrolytes have been generously supported by grants from Robert A. Welch Foundation (Grant F1599), the National Science Foundation (DMR-1721512). The authors acknowledge the Texas Advanced Computing Center (TACC) for the generous allocation of computing resources.

ORCID

Zidan Zhang https://orcid.org/0000-0002-6909-8742
Venkat Ganesan https://orcid.org/0000-0003-3899-5843

REFERENCES

[1] V. Ganesan, *Mol. Sys. Design Eng.* **2019**, *4*, 280.
[2] D. Mecerreyes, L. Porcarelli, N. Casado, *Macromol. Chem. Phys.* **2020**, *221*, 1900490.
[3] T. Y. Kim, H. W. Lee, M. Stoller, D. R. Dreyer, C. W. Bielawski, R. S. Ruoff, K. S. Suh, *ACS Nano.* **2011**, *5*, 436.
[4] Y. Wang, A. L. Agapov, F. Fan, K. Hong, X. Yu, J. Mays, A. P. Sokolov, *Phys. Rev. Lett.* **2012**, *108*, 88303.
[5] F. Fan, Y. Wang, T. Hong, M. F. Heres, T. Saito, A. P. Sokolov, *Macromolecules* **2015**, *48*, 4461.
[6] F. Fan, W. Wang, A. P. Holt, H. Feng, D. Uhrig, X. Lu, T. Hong, Y. Wang, N.-G. Kang, J. Mays, A. P. Sokolov, *Macromolecules* **2016**, *49*, 4557.
[7] F. Frenzel, R. Guterman, A. M. Anton, J. Yuan, F. Kremer, *Macromolecules* **2017**, *50*, 4022.
[8] P. J. Griffin, J. L. Freyer, N. Han, N. Geller, X. Yin, C. D. Gheewala, T. H. Lambert, L. M. Campos, K. I. Winey, *Macromolecules* **2018**, *51*, 1681.
[9] H. Ohno, K. Ito, *Chem. Lett.* **1998**, *27*, 751.
[10] H. Ohno, *Electrochim. Acta* **2001**, *46*, 1407.
[11] J. Yuan, D. Mecerreyes, M. Antonietti, *Prog. Polym. Sci.* **2013**, *38*, 1009.
[12] J.-H. Choi, Y. Ye, Y. A. Elabd, K. I. Winey, *Macromolecules* **2013**, *46*, 5290.
[13] A. S. Shaplov, D. O. Ponkratov, P.-H. Aubert, E. I. Lozinskaya, C. Plesse, F. Vidal, Y. S. Vygodskii, *Chem. Commun.* **2014**, *50*, 3191.
[14] Y. Yu, F. Lu, N. Sun, A. Wu, W. Pan, L. Zheng, *Soft Matter* **2018**, *14*, 6313.
[15] T. Huang, M.-C. Long, G. Wu, Y.-Z. Wang, X.-L. Wang, *ChemElectroChem* **2019**, *6*, 3674.
[16] N. Nishimura, H. Ohno, *Polymer* **2014**, *55*, 3289.
[17] N. S. Schauser, R. Seshadri, R. A. Segalman, *Mol. Syst. Des. Eng.* **2019**, *4*, 263.
[18] M. Forsyth, L. Porcarelli, X. Wang, N. Goujon, D. Mecerreyes, *Acc. Chem. Res.* **2019**, *52*, 686.
[19] X. Wang, R. Kerr, F. Chen, N. Goujon, J. M. Pringle, D. Mecerreyes, M. Forsyth, P. C. Howlett, *Adv. Mater.* **2020**, *32*, 1905219.
[20] Z. Zhang, B. K. Wheatle, J. Krajniak, J. R. Keith, V. Ganesan, *ACS Macro Lett.* **2020**, *9*, 84.
[21] R. L. Weber, Y. Ye, A. L. Schmitt, S. M. Banik, Y. A. Elabd, M. K. Mahanthappa, *Macromolecules* **2011**, *44*, 5727.
[22] Y. A. Elabd, M. A. Hickner, *Macromolecules* **2011**, *44*, 1.
[23] Y. Ye, J.-H. Choi, K. I. Winey, Y. A. Elabd, *Macromolecules* **2012**, *45*, 7027.

[24] A. E. Ozcam, N. Petzetakis, S. Silverman, A. K. Jha, N. P. Balsara, *Macromolecules* **2013**, *46*, 9652.
[25] O. Kim, G. Jo, Y. J. Park, S. Kim, M. J. Park, *J. Phys. Chem. Lett.* **2013**, *4*, 2111.
[26] R. Bouchet, S. Maria, R. Meziane, A. Aboulaich, L. Lienafa, J.-P. Bonnet, T. N. T. Phan, D. Bertin, D. Gigmes, D. Devaux, R. Denoyel, M. Armand, *Nat. Mater.* **2013**, *12*, 452.
[27] S. Inceoglu, A. A. Rojas, D. Devaux, X. C. Chen, G. M. Stone, N. P. Balsara, *ACS Macro Lett.* **2014**, *3*, 510.
[28] G. E. Sanoja, B. C. Popere, B. S. Beckingham, C. M. Evans, N. A. Lynd, R. A. Segalman, *Macromolecules* **2016**, *49*, 2216.
[29] Y. A. Elabd, *Mol. Syst. Des. Eng.* **2019**, *4*, 519.
[30] M. D. Galluzzo, W. S. Loo, E. Schaible, C. Zhu, N. P. Balsara, *ACS Appl. Mater. Interfaces* **2020**, *12*, 57421.
[31] T.-L. Chen, P. M. Lathrop, R. Sun, Y. A. Elabd, *Macromolecules* **2021**, *54*, 8780.
[32] M. P. Scott, C. S. Brazel, M. G. Benton, J. W. Mays, J. D. Holbrey, R. D. Rogers, *Chem. Commun.* **2002**, 1370. https://doi.org/10.1039/B204316P
[33] S. Mogurampelly, V. Ganesan, *Macromolecules* **2018**, *51*, 9471.
[34] H. Zhang, C. Liu, L. Zheng, W. Feng, Z. Zhou, J. Nie, *Electrochim. Acta* **2015**, *159*, 93.
[35] A. Wang, H. Xu, X. Liu, R. Gao, S. Wang, Q. Zhou, J. Chen, X. Liu, L. Zhang, *Polym. Chem.* **2017**, *8*, 3177.
[36] A. Wang, X. Liu, S. Wang, J. Chen, H. Xu, Q. Xing, L. Zhang, *Electrochim. Acta* **2018**, *276*, 184.
[37] J. L. Pablos, N. García, L. Garrido, F. Catalina, T. Corrales, P. Tiemblo, *J. Mater. Chem. A* **2018**, *6*, 11215.
[38] J. L. Pablos, N. García, L. Garrido, J. Guzmán, F. Catalina, T. Corrales, P. Tiemblo, *J. Membr. Sci.* **2018**, *545*, 133.
[39] M. Brinkkötter, E. I. Lozinskaya, D. O. Ponkratov, Y. Vygodskii, D. F. Schmidt, A. S. Shaplov, M. Schönhoff, *J. Phys. Chem. C* **2019**, *123*, 13225.
[40] A. Matsumoto, F. Del Giudice, R. Rotrattanadumrong, A. Q. Shen, *Macromolecules* **2019**, *52*, 2759.
[41] X. Wang, F. Chen, G. M. A. Girard, H. Zhu, D. R. MacFarlane, D. Mecerreyes, M. Armand, P. C. Howlett, M. Forsyth, *Joule* **2019**, *3*, 2687.
[42] A. Yokokoji, W. Kitayama, K. Wichai, O. Urakawa, A. Matsumoto, V. Vao-Soongnern, T. Inoue, *Polymers* **2021**, *13*, 1772.
[43] S. Mogurampelly, J. R. Keith, V. Ganesan, *J. Am. Chem. Soc.* **2017**, *139*, 9511.
[44] J. R. Keith, S. Mogurampelly, F. Aldukhi, B. K. Wheatle, V. Ganesan, *Phys. Chem. Chem. Phys.* **2017**, *19*, 29134.
[45] K. JRM, W. B. K. Santosh, G. Venkat, *J. Polym. Sci. B Polym. Phys.* **2017**, *55*, 1718.
[46] Z. Zhang, J. Krajniak, J. R. Keith, V. Ganesan, *ACS Macro Lett.* **2019**, *8*, 1096.
[47] J. R. Keith, N. J. Rebello, B. J. Cowen, V. Ganesan, *ACS Macro Lett.* **2019**, *8*, 387.
[48] J. R. Keith, V. Ganesan, *J. Chem. Phys.* **2019**, *151*, 124902.
[49] J. R. Keith, V. Ganesan, *J. Polym. Sci.* **2020**, *58*, 578.
[50] Z. Zhang, A. T. Nasrabadi, D. Aryal, V. Ganesan, *Macromolecules* **2020**, *53*, 6995.
[51] O. Borodin, G. D. Smith, O. Geiculescu, S. E. Creager, B. Hallac, D. DesMarteau, *J. Phys. Chem. B* **2006**, *110*, 24266.
[52] A. Maitra, A. Heuer, *Phys. Rev. Lett.* **2007**, *98*, 227802.
[53] D. Diddens, A. Heuer, O. Borodin, *Macromolecules* **2010**, *43*, 2028.
[54] V. Sethuraman, S. Mogurampelly, V. Ganesan, *Macromolecules* **2017**, *50*, 4542.
[55] V. Sethuraman, S. Mogurampelly, V. Ganesan, *Soft Matter* **2017**, *13*, 7793.
[56] M. P. Rosenwinkel, R. Andersson, J. Mindemark, M. Schönhoff, *J. Phys. Chem. C* **2020**, *124*, 23588.
[57] Z. Zhang, L. Wang, Z. Wang, X. He, Y. Chen, F. Mueller-Plathe, M. C. Boehm, *RSC Adv.* **2014**, *4*, 56625.
[58] J. Krajniak, S. Pandiyan, E. Nies, G. Samaey, *J. Chem. Theory Comput.* **2016**, *12*, 5549.
[59] J. Krajniak, Z. Zhang, S. Pandiyan, E. Nies, G. Samaey, *J. Comput. Chem.* **2018**, *39*, 648.
[60] Z. Zhang, J. Krajniak, G. Samaey, E. Nies, *Adv. Theory Simul.* **2019**, *2*, 1800102.
[61] Z. Zhang, J. Krajniak, V. Ganesan, *Macromolecules* **2021**, *54*, 4997.
[62] S. Pronk, S. Páll, R. Schulz, P. Larsson, P. Bjelkmar, R. Apostolov, M. R. Shirts, J. C. Smith, P. M. Kasson, D. van der Spoel, B. Hess, E. Lindahl, *Bioinformatics* **2013**, *29*, 845.
[63] W. L. Jorgensen, D. S. Maxwell, J. Tirado-Rives, *J. Am. Chem. Soc.* **1996**, *118*, 11225.
[64] A. D. Becke, *J. Chem. Phys.* **1993**, *98*, 5648.
[65] C. Lee, W. Yang, R. G. Parr, *Phys. Rev. B* **1988**, *37*, 785.
[66] R. Krishnan, J. S. Binkley, R. Seeger, J. A. Pople, *J. Chem. Phys.* **1980**, *72*, 650.
[67] M. J. Frisch, G. W. Trucks, H. B. Schlegel, G. E. Scuseria, M. A. Robb, J. R. Cheeseman, G. Scalmani, V. Barone, G. A. Petersson, H. Nakatsuji, et al., *Gaussian 09 Revision E.01* (2009), gaussian Inc. Wallingford CT.
[68] T. Lu, F. Chen, *J. Comput. Chem.* **2012**, *33*, 580.
[69] J. Zhang, T. Lu, *Phys. Chem. Chem. Phys.* **2021**, *23*, 20323.
[70] B. L. Bhargava, S. Balasubramanian, *J. Chem. Phys.* **2007**, *127*, 114510.
[71] N. Molinari, B. Kozinsky, *J. Phys. Chem. B* **2020**, *124*, 2676.
[72] G. S. Larsen, P. Lin, K. E. Hart, C. M. Colina, *Macromolecules* **2011**, *44*, 6944.
[73] K. E. Hart, L. J. Abbott, N. B. McKeown, C. M. Colina, *Macromolecules* **2013**, *46*, 5371.
[74] T. Darden, D. York, L. Pedersen, *J. Chem. Phys.* **1993**, *98*, 10089.
[75] G. Bussi, D. Donadio, M. Parrinello, *J. Chem. Phys.* **2007**, *126*, 14101.
[76] M. Parrinello, A. Rahman, *J. Appl. Phys.* **1981**, *52*, 7182.
[77] J. B. Haskins, W. R. Bennett, J. J. Wu, D. M. Hernández, O. Borodin, J. D. Monk, C. W. Bauschlicher, J. W. Lawson, *J. Phys. Chem. B* **2014**, *118*, 11295.
[78] A. T. Nasrabadi, V. Ganesan, *J. Phys. Chem. B* **2019**, *123*, 5588.
[79] H. Liu, X. Luo, A. P. Sokolov, S. J. Paddison, *J. Phys. Chem. B* **2021**, *125*, 372.
[80] C. J. F. Solano, S. Jeremias, E. Paillard, D. Beljonne, R. Lazzaroni, *J. Chem. Phys.* **2013**, *139*, 34502.

SUPPORTING INFORMATION

Additional supporting information may be found in the online version of the article at the publisher's website.

How to cite this article: Z. Zhang, D. Lin, V. Ganesan, *J. Polym. Sci.* **2022**, *60*(2), 199. https://doi.org/10.1002/pol.20210737